



Linking vegetation cover and seasonal thaw depths in interior Alaska permafrost terrains using remote sensing



John E. Anderson^{a,*}, Thomas A. Douglas^b, Robyn A. Barbato^c, Stephanie Saari^b, Jarrod D. Edwards^a, Robert M. Jones^c

^a US Army Geospatial Research Laboratory, Corbin Field Station 15315 Magnetic Lane, Woodford, VA 22580, United States

^b U.S. Army Cold Regions Research & Engineering Laboratory, PO Box 35170, Fort Wainwright, AK 99703, United States

^c U.S. Army Cold Regions Research and Engineering Laboratory, 72 Lyme Road, Hanover, NH 03755, United States

ARTICLE INFO

Edited by: Emilio Chuvieco

Keywords:

Hyperspectral imagery
Spectral reflectance
Permafrost
Vegetation
Seasonal thaw
Active layer
Classification

ABSTRACT

Permafrost in Interior Alaska is protected against summer thaw by an insulating layer of moss and mixed vegetative cover that regulates seasonal thaw and the end-of-summer season permafrost active layer depth. Thaw depths are laborious point scale measurements that can be difficult to translate regionally. Since disturbances are present on the landscape across many temporal and spatial scales they can greatly affect the soil and vegetation regime. Furthermore, many areas are denied full assessment due to terrain complexity or limited accessibility. As such, a remotely sensed means for estimating surface thaw based on insular vegetation composition would be advantageous. A synoptic evaluation of this insulating layer could eventually benefit regional mapping of areas where vegetation cover helps regulate thaw depths during the local growing season. Herein, we present multi-year data collected from three terrain types in Interior Alaska that relates seasonal thaw depth to vegetative cover type. Field samples for spectral reflectance, vegetation, soil, elevation and seasonal thaw depths were obtained from surveyed 1 m² quadrats during the local growing season (late July, each summer from 2014 to 2017) across three lowland boreal landscapes. Statistical relationships between vegetation and samples were explored using CCA and showed vegetative cover distributions were highly correlated in two dimensions with the principal variables represented almost evenly by the soil variable pH and thaw depth. Class maps representing vegetation and associated thaw depth were derived from hyperspectral imagery using field and imagery training data. Map accuracy assessment, conducted using random points to establish truth data, yielded overall accuracies of > 85%. Regression analysis and root mean square error testing of the predictive capacity of the vegetation classes and thaw depth was variable but encouraging, ranging from 5 to 11 cm or between an 8 and 37% chance of error. We feel the results are strong enough to stimulate more study in the evaluation of vegetation and thaw depth mapping during the local growing season.

1. Introduction

Discontinuous permafrost in Interior Alaska is “ecosystem protected” by an insulating surface layer of biomass, peat, and organic soils (Shur and Jorgenson, 2007). Mean annual temperatures in Interior Alaska, currently -1°C , are projected to increase 5°C over the next 80 years (Bouchard et al., 2016; Christensen et al., 2004; Chapman and Walsh, 2007; Douglas et al., 2014) and this is expected to initiate widespread permafrost degradation and alter hydrology, soils, vegetation, and microbial communities (Jorgenson et al., 2001a, 2001b; Walker et al., 2006; Mackelprang et al., 2017; Wilhelm et al., 2011; Wolken et al., 2011; Pastick et al., 2015; Fisher et al., 2018).

Temperature rise will also result in terrain changes from stable to transitional while increasing wetlands and open aquatic environments through disturbance, subsidence, thermokarst, and hydrologic changes (Brown et al., 2015; Douglas et al., 2016). These effects are translated in three ways: 1) as changes in vegetative cover, 2) deepening of the seasonally thawed “active layer” above permafrost, and/or 3) degradation of the underlying near surface permafrost. Christiansen et al. (2012) present data showing permafrost has generally warmed since the 1990s and a progressive increase in active layer thickness has been recorded in most regions with exceptions of northern Alaska and the western Canadian Arctic. Schuur et al. (2006) and Osterkamp et al. (2009) present dramatic evidence for the ramifications of these

* Corresponding author.

E-mail address: john.anderson@usace.army.mil (J.E. Anderson).

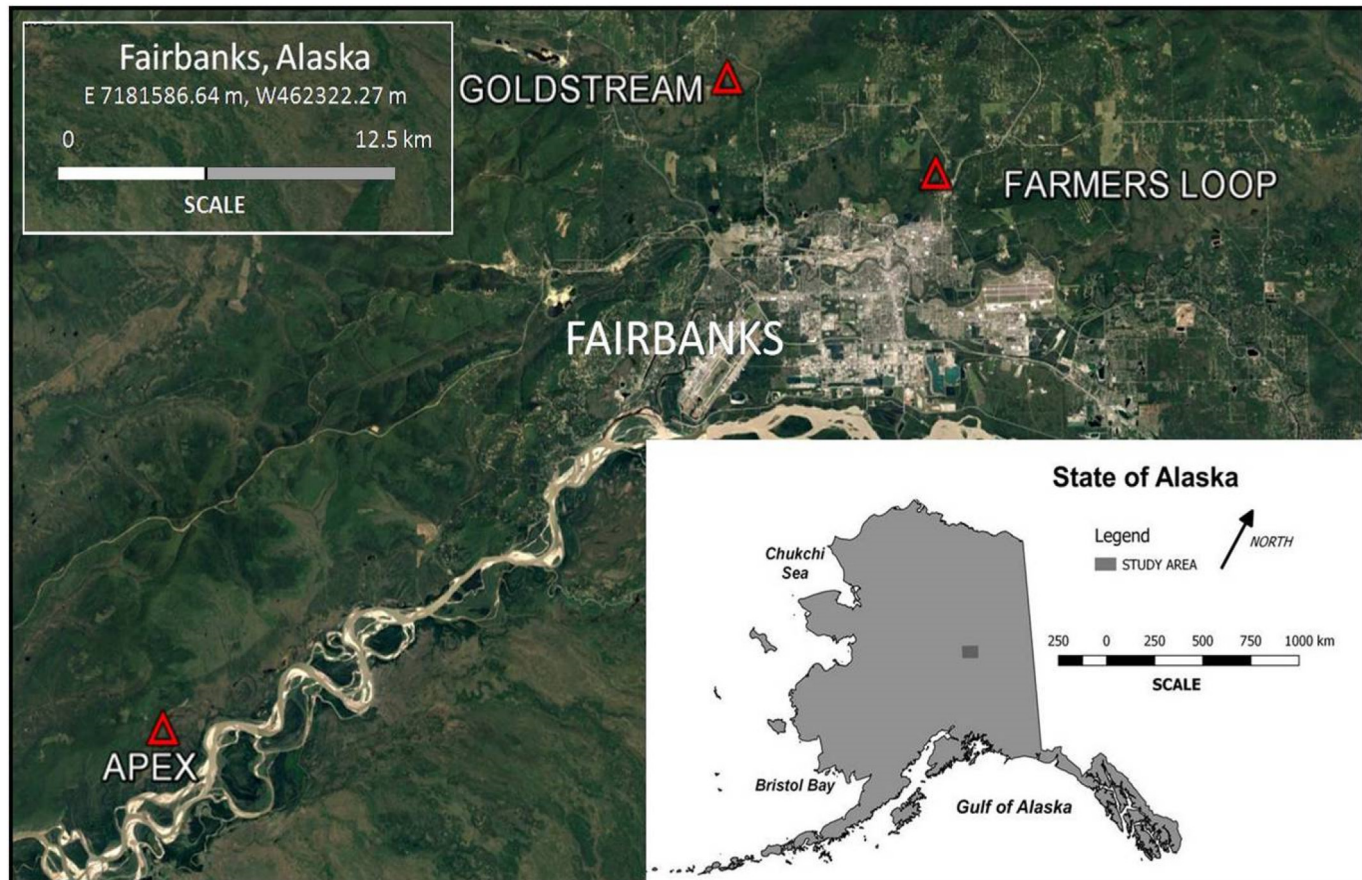


Fig. 1. Site locations for seasonal thaw depth study in Interior Alaska within the Chena River (Farmers Loop and Goldstream) and Tanana River (APEX) drainages.

transitions and the importance of vegetation stability in maintaining permafrost thaw depths where water-logged bogs are formed in regions of thaw nested among un-thawed areas of permafrost creating a heterogeneous mosaic of alternating stable and transitional vegetation terrain types. Finally, Walker et al. (2003) indicate water-logging to be the driving mechanism behind vegetation succession and subsequent changes in active layer thickness.

It has been demonstrated that vegetative processes are tightly coupled to hydrobiology and local soil micro flora that have the ability to adapt quickly to changing climatic conditions altering substrates and communities (Zak and Kling, 2006; Kuzyakov and Xu, 2013). Changes in permafrost extent and hydrobiology under a warmer climate regime have also been shown to influence vegetation species changes with shifts toward more aquatic wetlands and shrubs and away from boreal conifer and deciduous forests and ice-dominated terrain types (Xue et al., 2016; Shur and Jorgenson, 2007). The challenge in characterizing these dynamic changes is identifying and mapping the condition of permafrost thaw across the vast patchwork of sub-arctic and tundra landscapes to regionally depict (in) stability and transition of terrain state and identify areas vulnerable to thaw-induced changes. Landmark work in this area has combined aerial photography, large-scale satellite-based spectral imagery, and field measurements in continuous permafrost by Walker et al. (2003). That study, known as Arctic Transitions in the Land-Atmosphere System (McGuire et al., 2003), explored changes along a series of gradients to regionally characterize vegetation, soils and thaw depth across a vast northern ‘arctic bioclimate gradient.’

Building on this previous research, our objective is to explore current (in-season) relationships between the active thaw layer, elevation, soil, and vegetation type for three interior Alaska landscapes and apply this understanding as a foundation for mapping. In statistically relating vegetative cover types to field-based metrics, a mapping strategy is

emerging to spatially assess the general state of the active layer thaw and infer depth and terrain state (i.e., transitional or stable) using ground based and airborne multi- and hyperspectral reconnaissance methods. These methods have been shown to be effective at a variety of scales in terrain characterization, but few studies have attempted to link remotely sensed measurements with field metrics to help assess current thaw conditions and extent (Dingman and Koutz, 1974; McGuire et al., 2003; Morrissey et al., 1986; Peddle and Franklin, 1993; Jorgenson et al., 2001a, 2001b; Hachem et al., 2009; Jones et al., 2013; Kreig and Reger, 1982). In testing the ability to map seasonal thaw depth at higher resolutions, the spectral and spatial discrimination afforded by airborne hyperspectral imagery, combined with terrain elevation data obtained using a micro-unmanned aerial system (mUAS), was important to our study and expanded the capability to extrapolate information beyond local scales.

2. Materials and methods

Field measurements were made at road or trail-accessible sites near Fairbanks, Alaska and selected to represent a broad variety of interior Alaska ecosystems. Metrics were selected based upon the literature and were used to statistically explore the relationship between thaw depth and vegetation cover as well as drive the image classification. As such, a variety of biotic and abiotic measurements were collected. These measurements consisted of a rigorous vegetation survey to characterize the dominant vegetation types contained within each community, soil conditions, associated moisture and relevant biogeochemical attributes, thaw depth by frost probe and ground spectral attributes for each site. The methods are presented in detail below.

Table 1

Site geographic positions and designated Alaska vegetation classifications.

Site	Location (UTM 6N Easting/Northing, Elevation)	Attributes
USACE Farmers Loop Road Transect Length – 200 m 5 Quadrats (1m ²)	467727.975 m E, 7194711.221 m N 153.23 to 154.63 m (Ellipsoid)	Polygonal ground, open broadleaf and needle leaf forest, Mesic Graminoid Herbaceous and Tall Scrub. Permafrost depth avg. 58 cm. Plant diversity index 8.09 (by Shannon Index).
Goldstream Creek Transect Length – 300 m 5 Quadrats (1m ²)	459597.117 m E, 7198650.924 m N 191.43 to 193.53 m (Ellipsoid)	Intermittent polygonal ground with ponds, Mesic Graminoid – Bryoid Herbaceous with Needleleaf Woodland, some Open Low Scrub. Permafrost depth avg. 60 cm. Plant diversity index 5.46 (by Shannon Index).
APEX Transect Length – 500 m 5 Quadrats (1m ²)	436628.535 m E, 7174883.838 m N 130.89 to 131.57 m (Ellipsoid)	Perched water table and floating mat, Wet Graminoid – Bryoid Herbaceous, Closed Needleleaf Woodland Permafrost depth avg. 77 cm. Plant diversity index 4.68 (by Shannon Index).

2.1. Field sites

Three sites located in Interior Alaska near Fairbanks were used for this study: 1) the U.S. Army Corps of Engineers (USACE) Cold Regions Research and Engineering Laboratory's (CRREL) Farmers Loop Permafrost Experiment Station, 2) a field study site near Goldstream Creek within the Chena River drainage near Fairbanks, and 3) the Alaska Peatlands Experiment (APEX) site along the Tanana River lowlands southwest of Fairbanks (Fig. 1).

Each site represents a unique terrain type ranging from shallow active layer depths with ice wedge polygonal ground to deep active layers, quaking bogs (with shallow ponds) and perched water tables more consistent with ombrotrophic bogs. Site locations and attributes are shown in Table 1. The sites (transects and quadrats) were located and mapped using high precision GPS (global positioning system) by rapid-static method resulting in sub-centimeter accuracies. All survey data were placed in the WGS 84 horizontal datum in UTM Zone 6N coordinates using the NAVD 88 vertical datum. All units are in meters with final accuracies resulting in sub-centimeter values. Transects were initially established at each site using historical reconnaissance and photo-identifiable vegetation transitions as a guide. Transects ranged from 200 m at Farmers Loop Road to 500 m at APEX and were further refined using drone-based reconnaissance, photo interpretation and field surveys.

2.1.1. Vegetation sampling

The sites selected for this study represent a cross-section of the dominant land cover types in the lowland boreal areas of Alaska consistent with the USGS National Land Cover database (ref: <https://alaska.usgs.gov/science/program.php?pid=23>) and described by Viereck et al. (n.d.), for Alaska Vegetation Class Level III. Sampling quadrats were established along transects at 100 to 200 m intervals and sampled using a 1 m² frame template following methods described by Barbour et al. (1987). The area bounded by the template served as the minimum mapping unit for the imagery and map development (Fig. 2).

Vegetation was photographed and identified with cover estimates determined within 5 random ($n = 5$) 50 cm² subplots within each quadrat. Above ground biomass was also sampled by clipping vascular plants to the ground layer and cutting moss mats to the peat layer within the plots and prepared following the USDA – NRCS above ground biomass sampling procedure (Soil Survey Staff, 2009). The field vegetation sampling and analysis provided species composition, diversity and percent cover used to drive training data for image classification. The Shannon Index was used to compute and compare site diversity indices that provided a basis for the vegetation classes for each quadrat at each site following Brewer, 1979 and McPartland et al., 2019.

2.1.2. Soil biogeochemical measurements and active layer thaw depth sampling

Concurrent with the vegetation sampling, 20 cm peat (organic) core

samples were collected both inside and outside the quadrats for the purpose of obtaining pH, Eh (redoxomorphic) and gravimetric water content (GWC) (Table 2). Samples were placed on ice and processed within 4 h of sample collection. Peat samples were well mixed and water was added to each sample (1:1 soil:water) following methods prescribed by Eckert and Sims, 2011. After 1 min, the pH and Eh of each sample was recorded using a UB-10 bench top

probe (Denver Instrument, Bohemia, New York). Soil water content was determined gravimetrically (gravimetric water content-GWC) with a 10 g subsample of the bulk soil dried at 105 °C for 24 h. GWC was reported as a percent mass of water in the peat sample. Data were compared in JMP11 (SAS, Cary, NC) using analysis of variance. Means were compared using an all pairs Tukey honestly significantly different (HSD) test. In the field, active layer thaw depths were collected with a 2.5 m long, 1 cm diameter graduated metal rod ("frost probe") that was pushed vertically downward into the ground to refusal following established methods described by Douglas et al. (2016). Thaw depths were measured in late July 2014 to 2017 (summer season thaw during peak vegetation green-up) at multiple areas within each quadrat ($n = 10$). These data were used in a multivariate, direct gradient analysis to explore associations between the plant compositions and thaw depth measurements.

2.1.3. Field spectroradiometry of vegetation

Spectral signatures were acquired concurrent to airborne missions at each site within the quadrats to facilitate training development and spectral matching for the classification process. An SVC HR-1024i (Spectra Vista Corporation, Poughkeepsie, NY) spectroradiometer (350 to 2500 nm) was used to collect reflectance data in full sunlight at a distance of 1 m nadir above the ground target and (reflectance) calibration was performed by measuring Spectralon (NIST) (white) standard following Satterwhite and Henley (1990).

Spectral resolution for the instrument is ≤ 3.3 nm (FWHM) VNIR region and ≤ 10 nm (FWHM) in the SWIR. The nominal field-of-view of the SVC instrument is $\frac{1}{4}$ allowing a sample diameter of approximately 7 cm to be recorded. Ten spectra were acquired and averaged for each of the 5 sub-plots sampled to provide signatures representing (quadrat) vegetation composition as well as homogenous (endmember) targets representing light and dark-toned soils based on methods described by Perry et al. (2000). Spectral reflectance data were normalized using methods described by Smith et al. (1985) and Sasaki et al. (1983) where the suppression of albedo effects can be achieved by dividing the reflectance of all wavelengths by the mean of all reflectance at all wavelengths in each field sample. Finally, spectral signatures and end-members collected for the field sites were compiled into libraries and used in the reflectance-calibration of the hyperspectral images.

2.2. Airborne imagery acquisitions and analytical product generation

Two sources of imagery data were used in our research: first, a fixed-wing, EBEE micro-UAS by Sensefly, Geneve, Switzerland



Fig. 2. Ground photos of vegetation associated with the study sites: A) USACE CRREL Farmers Loop Mesic Graminoid Herbaceous-tussock cotton grass (*Eriophorum vaginatum*) and sample template, B) Shrub layer (*Betula nana*) with Black Spruce (*Picea mariana*), C) Goldstream Creek Wet Graminoid and Bryoid Herbaceous w/ Closed Needle Leaf Woodland and Open Low Scrub - moss, sedge and bush cinquefoil (*Sphagnum*, *Carex* sp. and *Potentilla* sp.), D) APEX Mesic Graminoid and Bryoid Herbaceous and Open Needle Leaf Woodland w/ Tall and Low Scrub - Bluejoint reedgrass, sedge and black spruce (*Calamagrostis* sp., *Carex* sp., and *Picea mariana*).

Table 2

Site and quadrat descriptions and soil properties from each site with average and standard error of five replicates.

	pH	Eh (mV)	Gravimetric water content (%)
Farmers loop - Mesic Graminoid site			
Q1 Tussock cotton grass, Dwarf birch	6.2 (0.2)	36.0 (9.6)	82.4 (1.9)
Q2 Tussock cotton grass, Bluejoint reedgrass	6.5 (0.1)	19.6 (5.4)	89.6 (0.9)
Q3 Tussock cotton grass, Bluejoint reedgrass	6.7 (0.1)	7.8 (3.3)	85.8 (1.1)
Q4 Tussock cotton grass, Bluejoint reedgrass, Dwarf birch	6.6 (0.1)	18.2 (5.4)	86.2 (3.3)
Q5 Bluejoint reedgrass, Dwarf birch	6.7 (0.1)	9.2 (3.4)	86.3 (0.9)
Goldstream Creek - Mesic Graminoid-Bryoid site			
Q1 Narrowleaf lab. Tea, Moss, Bog rosemary	4.5 (0.3)	137.2 (19.3)	88.3 (1.6)
Q2 Moss, Tussock cotton grass	4.1 (0.1)	158.4 (3.9)	90.4 (0.8)
Q3 Tussock cotton grass, Blueberry	5.2 (0.1)	94.4 (4.9)	89.5 (2.1)
Q4 Blueberry, lowbush cranberry	4.8 (0.1)	114.6 (5.2)	82.6 (4.6)
Q5 Bluejoint reedgrass	4.8 (0.1)	117.4 (7.0)	94.4 (0.3)
APEX - Wet Graminoid-Bryoid site			
Q1 Moss, black spruce	5.6 (0.1)	75.4 (7.5)	87.8 (3.2)
Q2 Moss, Bog rosemary, Blueberry	5.2 (0.2)	94.8 (10.1)	93.6 (0.5)
Q3 Moss, Alaska Cotton grass	4.7 (0.0)	122.6 (2.5)	93.2 (0.1)
Q4 Silvery sedge	4.8 (0.0)	117.2 (2.5)	92.5 (0.5)
Q5 Moss, Bog rosemary, Tamarack	4.7 (0.1)	121.8 (5.0)	93.6 (0.5)
	$P < 0.0001$	$P < 0.0001$	$P < 0.0001$

possessing a near IR, non-metric camera payload (Canon S110 - 3 channel NIR) and second, a commercial airborne hyperspectral imager the ProSpecTIR™ VNIR SWIR pushbroom imaging spectrometer (400 to 2450 nm in 360 channels, nominal resolution 10 nm) operated by SpectIR Corp. of Reno, Nevada.

Near infrared imagery (5 cm GSD) of all the sites was acquired by the EBEE drone to create high resolution digital terrain elevation models (DTMs) used to establish transects, quadrats and as an environmental variable in the direct gradient statistical analysis. The data (300 to 400 imagery frames per site) were photogrammetrically processed using ground-surveyed calibration targets to produce textured point clouds, DTMs, and orthorectified images using AGISOFT Photoscan (St. Petersburg, Russia) rectification software. The DTMs produced from the EBEE missions were generated from a

photogrammetrically-derived point cloud and subsequently used to rectify and refine the positional geometry of the hyperspectral data.

The SpectIR hyperspectral imager was deployed during the July 2014 sampling season and provided data at a pixel resolution of 1 m ground sample distance (GSD). Image data from the hyperspectral mission was processed to (percent) reflectance units in ENVI format to facilitate spectral matching and training sample development. This was accomplished by matching the field spectral measurements for vegetation composition and endmembers of the targets to their respective image locations using the Empirical Line Calibrat [Jensen et al. \(2007\)](#) ion (ELC) method described by, [Karpouzli and Malthus \(2003\)](#) and [Smith and Milton \(1999\)](#) within the OPTICKS Spectral Processing program ([Ball Aerospace, 2008](#)). ELC was selected based on its efficient estimate of surface reflectance and low error in the resulting

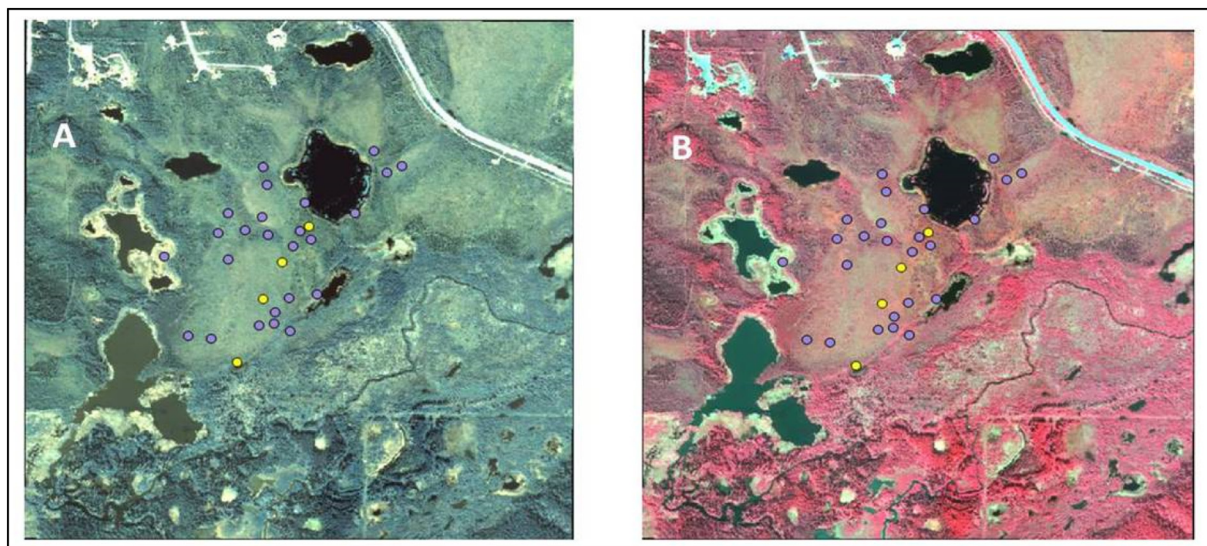


Fig. 3. Imagery and derived products (clock-wise from left) A) ProSpectIR hyperspectral data for Goldstream Creek – Bands 65–55–40 RGB (590 nm, 560 nm, 515 nm) and B) – Bands 90–55–30 RGB (770 nm, 670 nm, 485 nm) showing sample quadrats (yellow dots) and random check points (purple dots). (For interpretation of the references to color in this figure legend, the reader is referred to the web version of this article.)

calibration.

Examples of the hyperspectral data are presented in Fig. 3 for the Goldstream Creek site and show the location of the sample quadrats (yellow) and random ground truth check points (purple) in Figs. A and B.

2.2.1. Image and spectral processing

Hyperspectral imagery, geospatial layers (e.g., shapefiles) and spectral reflectance data were entered into the Quantum Geographic Information System (ver. Nodebo 2.16) – QGIS and saved as project files. The signature processing, training data extraction, training sample analysis resulting classifications, and error analyses were executed with QGIS using the Semi-Automatic Classification Plug-in or SCP developed by Luca Congedo (2016). SCP allows ingestion, exploitation and analysis of multiband data and spectral signatures along with several robust classifiers including the Spectral Angle Mapper (SAM) algorithm used with our data sets. SAM is an automated method for comparing image spectra to individual or library spectral data and assumes that the data have been reduced to *apparent* reflectance (e.g., atmospherically corrected). The algorithm determines spectral similarity by calculating the angle between them by treating them as vectors in a space dimensionally equal to the number of bands in the data set (Kruse et al., 1993). The inputs to the SAM classifier were training areas developed from the hyperspectral imagery for our quadrats at each site.

2.2.2. Hyperspectral training sample selection and thaw depth mapping

Vegetation maps and associated with thaw depths were developed for each site based on training samples extracted from the site quadrats (Sluiter and Pebesma, 2010). ProSpectIR hyperspectral imagery data (360 bands – 360 nm to 2400 nm) were loaded into QGIS and exploited using the SCP plug-in for spectral analysis and classification.

Training samples were delineated from each quadrat at each of the three sites using the region of interest (ROI) tool in SCP (Fig. 4). Once collected, training samples were assigned to classes reflecting the dominant vegetation cover type and associated thaw depth.

The area extracted for each ROI was centered on the control point for each quadrat and covered 2 m² in area, encompassing the quadrat and some area outside. This assured the sample area was completely represented in the training statistic. Prior to running the SAM classifier, spectral signatures were generated for each training sample and analyzed for statistical separation using the spectral angle method (Kruse

et al., 1993) The spectral angle method returns results for training sample scores where 0 is identical (same feature) and 180 represents samples that are completely different (different feature). Once the separation analysis was concluded the training samples were submitted to the SAM classifier. SAM is discrete and based on the measurement of the similarity between two spectra for a given feature across all bands. This similarity can be obtained by considering each spectrum as a vector in q-dimensional space, where q is the number of bands. The algorithm determines the spectral similarity between two spectra by calculating the angle between the two spectra, treating them as vectors in a space with dimensionality equal to the number of bands. Resulting classifications were checked for accuracy using errors of omission and commission as described by Campbell and Wynne (2011). During the July 2017 sampling period a truth data map was produced for each site by re-sampling the quadrats and collecting ten thaw depth and vegetation cover data points from an additional twenty-five random locations within a 1 km radius around the established sample quadrats. Following Congalton (1991), this provided multiple samples associated with each training class to be used in the error analysis for map accuracy. The resulting map was used with SCP to generate a pixel accuracy assessment for each site.

2.3. Statistical analysis

The relationship between sampled vegetation composition and measured site environmental variables was explored using multivariate direct gradient analysis. Following procedures developed by Ter Braak (1986), Canonical Correspondence Analysis (CCA) was used to identify relationships between vegetation composition/distribution and environmental factors, dependent variables and uncorrelated, independent variables (e.g., pH, Eh, permafrost depth, elevation, and gravimetric water content-GWC). CCA is widely accepted as a multivariate method of choice when relating biotic and abiotic factors where natural or anthropogenic influences drive species distribution (Jongman et al., 1986). As a tool to explore the influence of the environment on species, CCA produces scores as weighted averages and results in axes with scales representing a set of standardized scores. This technique has been used for over 25 years in the analysis of biotic and abiotic relationships (Ter Braak, 1986; Kuuluvainen et al., 1993; Marschner et al., 2001; Drenovsky et al., 2004; Dumbrell et al., 2010). While similar to principle components analysis, CCA draws from two

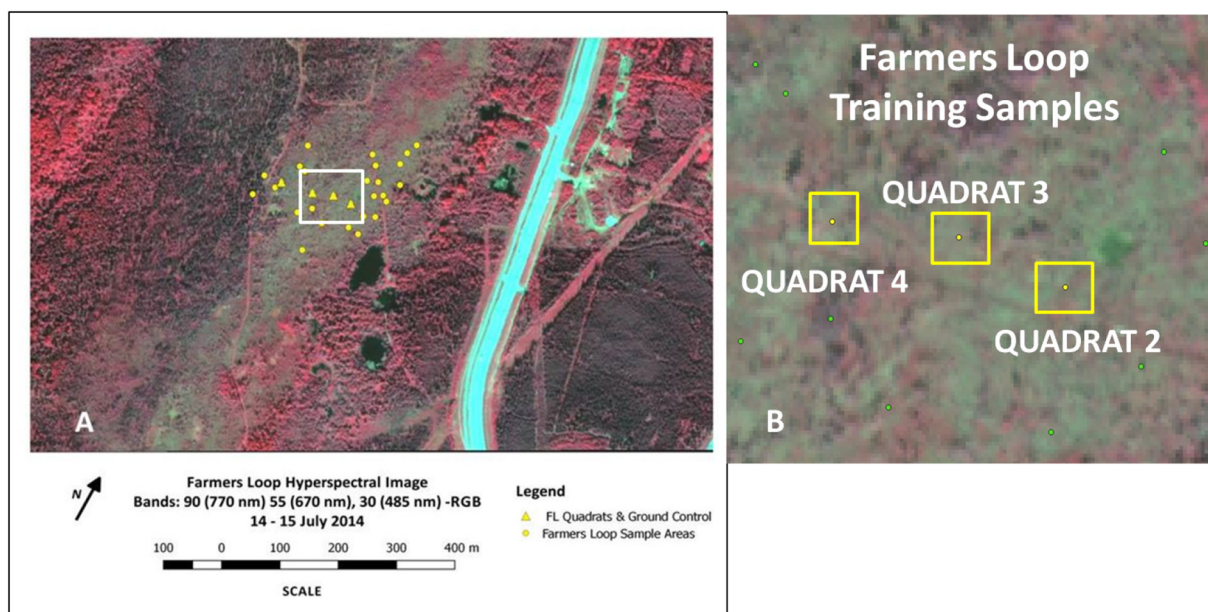


Fig. 4. A) ProSpectIR hyperspectral false color data for Farmers Loop – Bands 90–55–30 RGB (770 nm, 670 nm, 485 nm) and B) Training sample locations for quadrats 2, 3, and 4.

different multivariate distributions (in our case field measurements for vegetation species types and abiotic metrics). CCA's value is that resulting analytical scoring and graphical presentation reflect how species (or communities) of organisms being studied may cluster or overlap as environmental variables influence pattern distributions and associations. Generally, the length of the vector line designates the influence of the abiotic variable. All analyses were performed using the open source PAST v3.14 multivariate statistical package (Øyvind Hammer, Natural History Museum, University of Oslo). Effective ordinations result in defined variance in a community matrix and fix a score that is attributed to a particular measure of importance that reflects: 1) the combined effect of environmental variables and (in this case) vegetation and 2) the interest score reflecting the significance of the relationship between two particular variables. For our data, several iterations were generated using data combined from the year-to-year sampling. This allowed vegetation cover and (the most influential) environmental measurements to be explored and isolated. Finally, while the vegetation classes and ancillary variables including thaw depth were statistically explored using CCA, we tested the measured and map-predicted thaw depths based on 25 random check points established around each site using linear regression, generating an r-square and RMSE for each resulting site model.

3. Results

3.1. Vegetation, soils, and seasonal thaw

Measurements at each site obtained from the sampling quadrats showed distinct differences in vegetation, soils, and mid-summer thaw depths for each community. Overall, the Farmers Loop soils had significantly ($p < 0.0001$) higher pH and slightly lower gravimetric water content than the soils at the Goldstream and APEX sites (Table 2). Eh was also significantly ($p < 0.0001$) lower in the pore water of the soils from Farmers Loop. Information derived from the vegetation sampling (important to the mapping goals of the project) showed differences in composition and cover. At the Farmers Loop site vegetation was classified as Mesic Graminoid Herbaceous with Open Broadleaf and Needle Leaf Forest with Closed Tall Scrub. Vegetation was primarily dominated by tussock cotton grass and bluejoint reedgrass with twenty-seven other species identified on highly dissected, ice wedge polygonal ground with

some standing water.

The Farmers Loop site also possessed soil redoxomorphic characteristics that were more neutral (average pH 6.5) but with higher reducing conditions (average Eh 18.6 mV) than either the Goldstream or APEX sites. Gravimetric water content (GWC) averaged 86.06% for soils sampled within the quadrats and seasonal thaw depths as of July (2014–2017) at Farmers Loop averaged 56.39 cm with a standard deviation of 8.97. Thaw depths measured for all sites across the sampling period are shown in Fig. 5 along with the trends across all quadrats.

The Goldstream site was classified as Mesic Graminoid and Bryoid Herbaceous and Open Needle Leaf Woodland with Tall and Low Scrub. Also classified at Goldstream were numerous Aquatic Herbaceous open freshwater areas. The Goldstream site was dominated by moss, tussock cotton grass, bluejoint reedgrass and blueberry with twelve other species also recorded. Soil characteristics for the Goldstream site included lower (acidic) pH values that averaged 4.67 and more oxidizing conditions with Eh values averaging 124.40 mV. GWC data for soils at Goldstream averaged 88% similar to Farmers Loop. The July seasonal thaw depths to the top of near surface permafrost ranged from 38 cm to 87 cm with an average of 56 cm and a standard deviation of 13 cm.

APEX represented the wettest site of the three (average GWC – 90%) and was classified as Wet Graminoid and Bryoid Herbaceous with Closed Needle Leaf Woodland and Open Low Scrub. The APEX site consisted of closed forested margins surrounding a floating bog and mat over a perched water table close to the Tanana River drainage marked by numerous oxbow lake scars with thirteen other minor species enumerated. This site had an average soil GWC of 92.14% with an acidic pH of 5.0 and more oxidized conditions with an Eh of 106.36 mV. The vegetation composition at APEX was dominated by sphagnum moss and silvery sedge with thirteen other minor species enumerated. The site had an average soil GWC of 92.14% with an acidic pH of 5.0 and more oxidized conditions with an Eh of 106.36 mV. The July seasonal thaw depths for APEX were the deepest of all the sites, averaging 83 cm with a standard deviation of 13.2, deeper than Farmers Loop and slightly deeper than Goldstream.

3.2. Spectral reflectance data

The resulting spectra are presented in Fig. 6 for each site with the dominant vegetation cover type associated with the indicated spectrum.

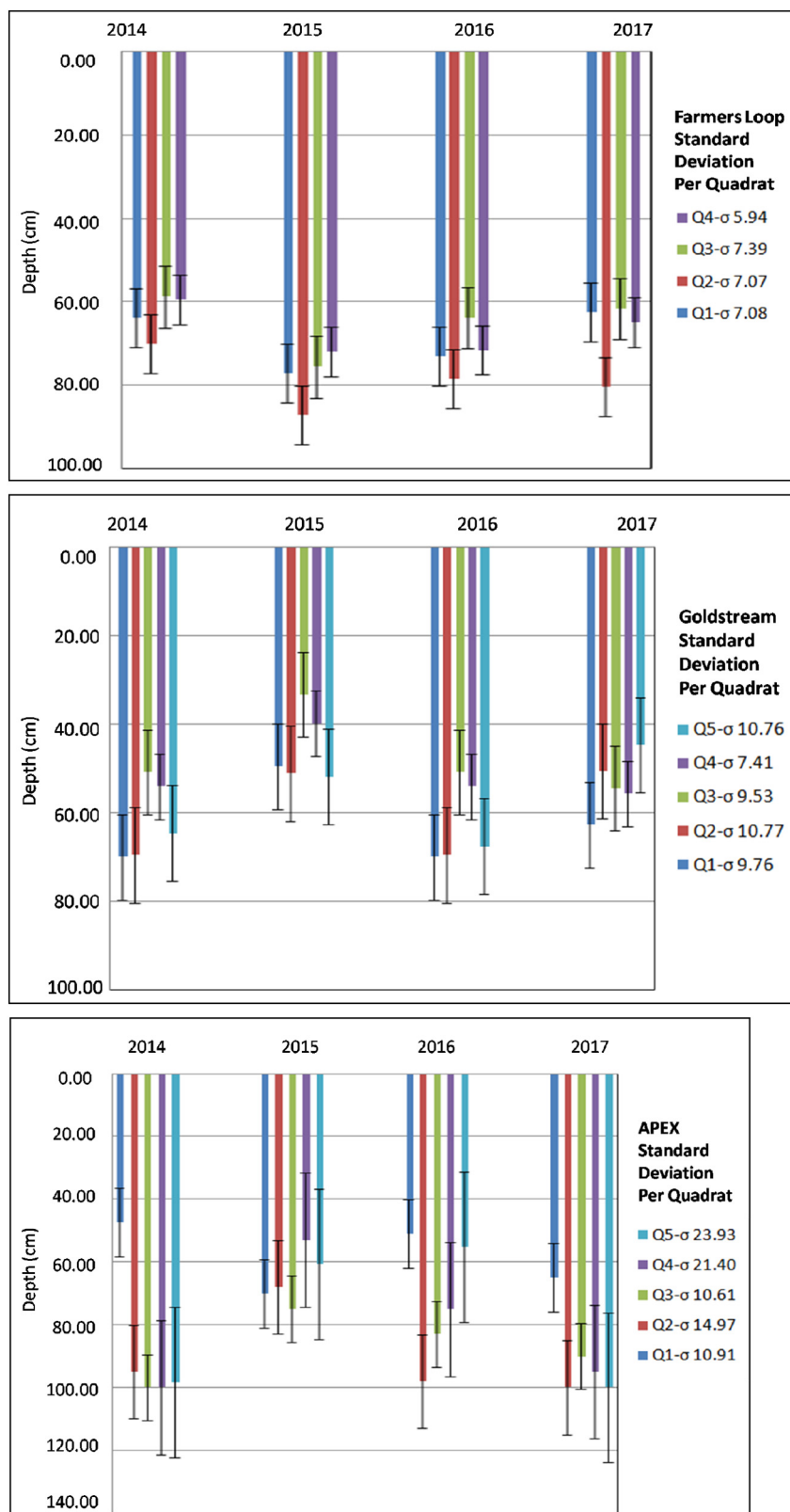


Fig. 5. All thaw depths and trends plotted for the sampling period July 2014–2017 for Farmers Loop, Goldstream and APEX.

At Farmers Loop (Mesic Graminoid Herbaceous) vegetative cover was dominated by tussock cotton grass, paper and dwarf birch (*Betula neoalaskana* and *B. nana*) and bluejoint reedgrass in all quadrats (> 50% cover) followed by minor mixtures of pacific willow (*Salix lasiandra*), blueberry (*Vaccinium uliginosum*), marsh five finger

(*Potentilla palustris*) and Labrador tea (*Ledum groenlandicum*).

The polygonal ground at Farmers Loop possessed some open areas of wet peat and standing water that were present between tussocks each year serving to reduce reflectance as seen in the spectrum for Quadrat 1 as well as deepen the spectral water absorption bands.

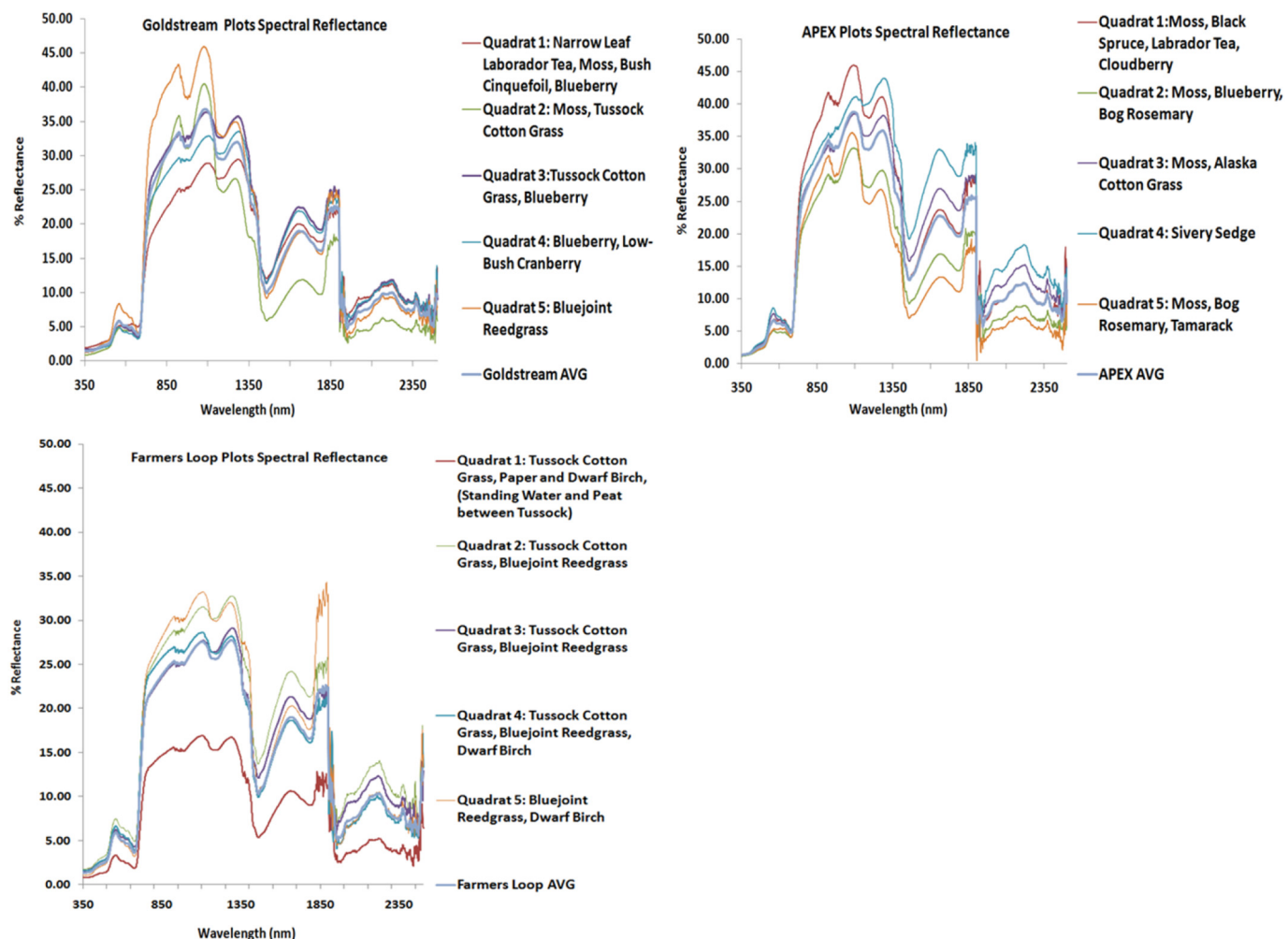


Fig. 6. (Clockwise from top right) Catalog spectral reflectance of dominant cover types (> 50% cover in the FOV) identified for Goldstream Creek, APEX and Farmers Loop quadrats with the average site spectra also presented.

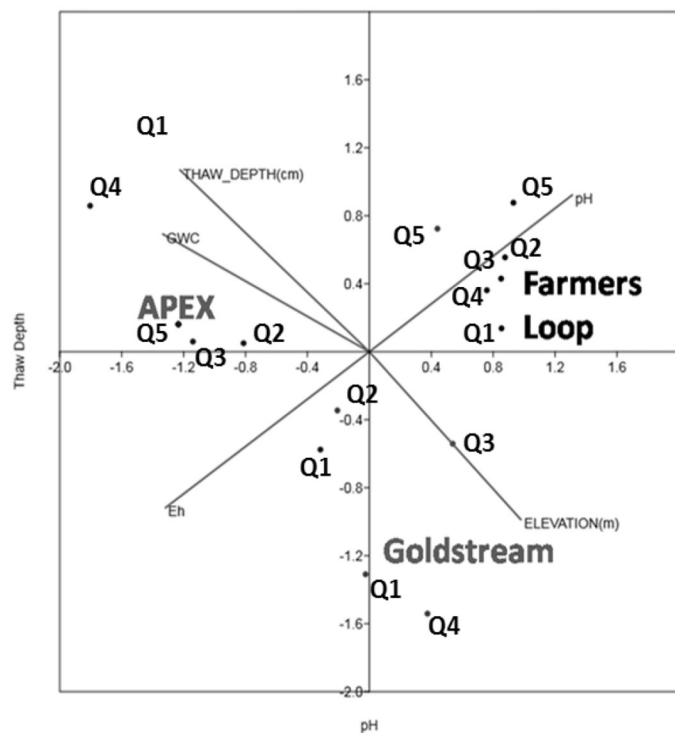
Reflectance spectra acquired for the Goldstream quadrats (Mesic Graminoid and Bryoid Herbaceous) were dominated by bluejoint reedgrass and moss (*Sphagnum sp.*) (> 70% cover) with a mixture of blueberry, tussock cotton grass, narrow-leaf Labrador tea (*Ledum decumbens*), lowbush cranberry (*Vaccinium vitis-idaea*), and bush cinquefoil (*Potentilla fruticosa*). Sample quadrats at Goldstream were established adjacent to a pond (quadrat 1) and then moved across a dome (quadrats 2 to 4) and then lower to another small pond. These plots had fewer openings between tussocks and generally were less saturated with fewer bare areas of wet peat, as seen at Farmers Loop. Spectral reflectance data from APEX was dominated by silvery sedge (*Carex canescens*), moss and bog rosemary (*Andromeda polifolia*) vegetative cover (70 to 100%) followed by Alaska cotton grass (*Eriophorum scheuchzeri*), Tamarack (*Larix laricina*), Labrador tea, and black spruce (*Picea mariana*). APEX quadrats 2, 3, and 4 occupied a floating mat situated on a perched water table completely covered with vegetation and no standing water or pools and quadrats 1 and 5 were situated in closed woodland areas. The spectral data provided guidance from the standpoint of imagery band selection, class development and signature separation with the near IR (750 to 1300 nm) and the SWIR (1440 to 1740 nm) exhibiting good separation between most of the cover types *within* the sites. Separation between the sites themselves is achieved in the SWIR (1000 to 1400 nm) as shown in the averaged spectrum.

3.3. Abiotic drivers of vegetation composition

Vegetation species and percent cover were described and related to environmental variables using CCA in the computer program PAST. For the three sites studied, 30 cover species and five environmental variables were evaluated including: soil pH (log of the hydrogen ion), soil Eh (in mv), soil GWC (% of mass), elevation (m) and July seasonal thaw depth of permafrost (cm). The goal of CCA was to determine which physical and environmental variable(s) most strongly related to the distribution of the vegetative cover types. Environmental variables were selected as part of related studies of permafrost dynamics and for their strong association with growing conditions typically found in (wetland) bog terrain types (Mitch and Gosselink, 1986). As described in the Methods, CCA was used prior to map development to test the use of vegetative cover as a surrogate metric of seasonal thaw depth distributions during the growing season by analyzing the strength of the relationship(s) vegetation communities have with the sampled metrics. The sensing literature abounds with research on the control soils and ancillary variables exert over vegetation community patterns with data such as Duguay et al.'s (2005) work presenting relationships derived using moderate to high spatial resolution global remote sensor data and microwaves.

Our CCA ordination showed distinct separation of the three sites reflecting their independent and diverse terrain and vegetation species compositions (Fig. 7). The influential environmental variables are plotted as vectors originating from the plot origin and the axes

Site Distribution and Environmental Variables



Vegetation Zones and Environmental Variables

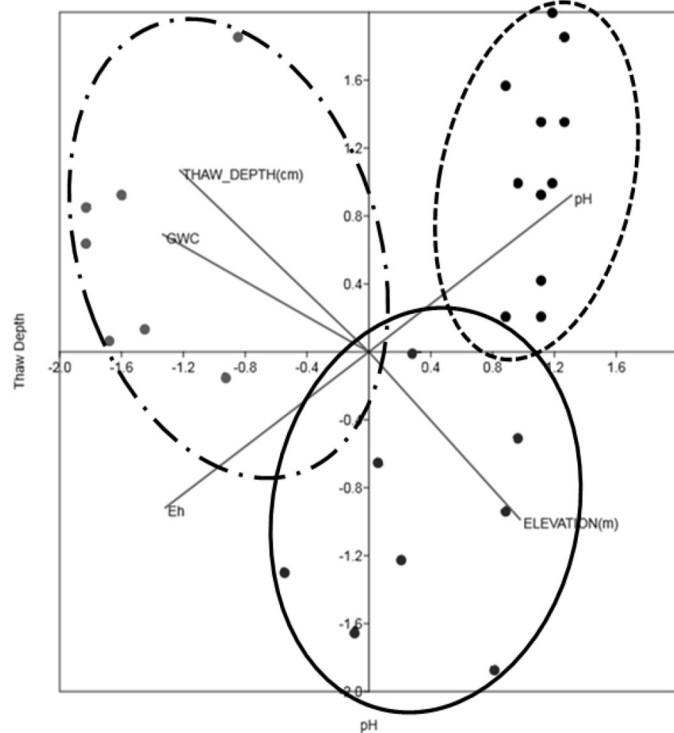


Fig. 7. CCA plots showing (left) environmental variables, sites and quadrats and (right) relationships between species sampled and the three vegetation zones representing: Mesic graminoid herbaceous (small dash line -Farmers Loop), Mesic graminoid-bryoid herbaceous w/ needleleaf woodland and low scrub (solid line-Goldstream Cr.), and Wet graminoid-bryoid herbaceous (dash/dot line-APEX). Dots associated with the ‘Vegetation Zones’ plot represent the distribution of dominant vegetation types.

represent the correlation scores for the strongest variables (e.g., pH and thaw depth). Measurements from the Farmers Loop and APEX sites broke along clear lines with tight groupings for the sample quadrats while variables at the Goldstream site exhibited a broader continuum with the sites having greater spacing due to a more varied cover and composition (Anderson et al., 2016).

The CCA resulted in two variables explaining over 70% of the variance of the data. Among the variables evaluated, pH was the major correlate at 42% with the x-axis of the CCA having the greatest influence on vegetation composition from the standpoint of soil substrate condition (Tables 3A & B).

Soil redox conditions are very closely related to plant stress and plant zonation (Moore and Bellamy, 1974). A negative correlation between Eh and pH was observed for each site, as is common to all soils (Bohrerova et al., 2004; Husson, 2013; Anderson et al., 2016). Low

redox condition is an indicator of anaerobic conditions, which is particularly important in Alaskan wetlands where soil hydrology impacts vegetation composition and health. Measurements showed Farmers Loop being the most neutral of the sites with Goldstream and APEX exhibiting more acidic soil conditions. This observed relationships between pH and vegetation is important and has been established at other permafrost sites as well as historically studied as a controlling factor in soil and vegetation community development in wetlands (Gorham, 1967; Hodgkins et al., 2014).

Next, thaw depth emerged as the major correlate aligned with the y-axis dividing the plant species into two distinct groups clustered around each site. Although the summary values placed thaw depth second at 38% of the variance when considered with the other variables, the resulting correlations with vegetation species are quite high at 0.88. In addition, interset correlation for this variable is also strong at 0.54.

Table 3

A and B CCA summary statistics for vegetation species composition for Farmers Loop, Goldstream and APEX sites and the environmental variables from Fig. 7: Eigenvalues species-environmental variable correlations, and interset correlations.

Table 3A. summary	Axis 1	Axis 2
Eigenvalues	0.733	0.392
Percentage	41.9	38.01
Spec.-env. correlations	0.979	0.883

Table 3B. Interset correlations between environmental variables and site scores

Variables	Envi. axis 1	Envi. axis 2
Gravimetric Water Content	-0.659	0.348
pH	0.666	0.442
Eh	-0.669	-0.441
ELEV (m)	0.470	-0.536
T_DEPTH (cm)	-0.595	0.544

Species identified as largely facultative wetland and obligate wetland aligned with APEX, the wettest site possessing the deepest seasonal thaw and end of season active layer depths. The drier sites- Farmers Loop and Goldstream- possessed vegetation in both *facultative* and *facultative-wet* wetland vegetation categories as described by Cowardin et al. (1979) (ref: www.wetland-plants.usace.army.mil) and exhibited shallower thaw depth measurements.

It is interesting to note that although GWC, elevation and Eh did not relate strongly to the first few axes, these variables do account for some of the remaining variation and their positions on the plots follow distinct patterns. As mentioned, Eh is inversely related to pH which is common in wetland environments where soil acidity and anoxic/reddoxomorphic soil characteristics are anti-correlated (Bohrerova et al., 2004; Husson, 2013). Additionally, thaw depth and elevation are opposed in the plot suggesting a relationship between permafrost and topographic position on the landscape with the low lying, low gradient APEX site having the most areal extent of standing water. Finally, GWC's position near thaw depth suggests a logical relationship between these two variables as a soil moisture contribution to seasonal thaw.

3.4. Hyperspectral training sample selection and thaw depth mapping

Fig. 8 presents examples of extracted image spectra for quadrat training samples from Farmers Loop. Signature separation scores are shown in Table 4 for the number of classes representing the sample quadrats at all sites. The resulting statistical separation between the classes was good to fair with scores ranging between 18.975 for APEX to 34.059 for Goldstream. Lower scores were due in part to cover and compositional similarities and were anticipated in the analysis. Fig. 9 A-C present the vegetation and thaw depth estimate maps based on the July 2014 imagery data. Each map shows strong vegetation zonation associated with thaw depths collected from July 2014 to 2017 as well as the sample quadrat locations.

Table 4
Signature separation scores for site classes.

Site	No. of map classes	Spectral angle - separability score
USACE Farmers Loop	6	27.848
Goldstream Creek	7	34.059
APEX	5	18.975

3.5. Accuracy assessment of vegetation maps and thaw depth estimates

During the July 2017 sampling period a truth data map was produced for each site by re-sampling the quadrats and collecting ten thaw depth and vegetation cover data points from an additional twenty-five random locations within a 1 km radius around the established sample quadrats. Following Congalton (1991), this provided multiple samples associated with each training class to be used in the error analysis for map accuracy. The resulting map was used with SCP to generate a pixel accuracy assessment for each site with overall accuracies of: 87% at Farmers Loop, 86% at Goldstream Creek, and 85% at APEX. While the vegetation classes and thaw depths were related statistically for the three regions, we tested the measured and map-predicted thaw depths based on 25 random check points established around each site. Fig. 10A-C shows the resulting regression plots for each site with the model, r-square and RMSE provided. Table 5 provides a summary of the model results per site between map-predicted and measured field values.

Farmers Loop offered the driest and most complex terrain featuring strongly dissected ground resulting from a patchwork of tussock sedges and cotton grass with low shrubs. In aerial imagery, the tussock area at Farmers Loop exhibited classic ice-wedge polygonal terrain exhibiting shallow (up to 50 cm), low lying troughs between the elevated tussock mounds containing some standing water with grass and bare organic material. This area possessed the shallowest permafrost seasonal thaw depths recorded across the three years of summer sampling.

This suggests the vegetation and soil conditions in the tussock terrain possessed more insulative value; preserving shallow thaw depths in

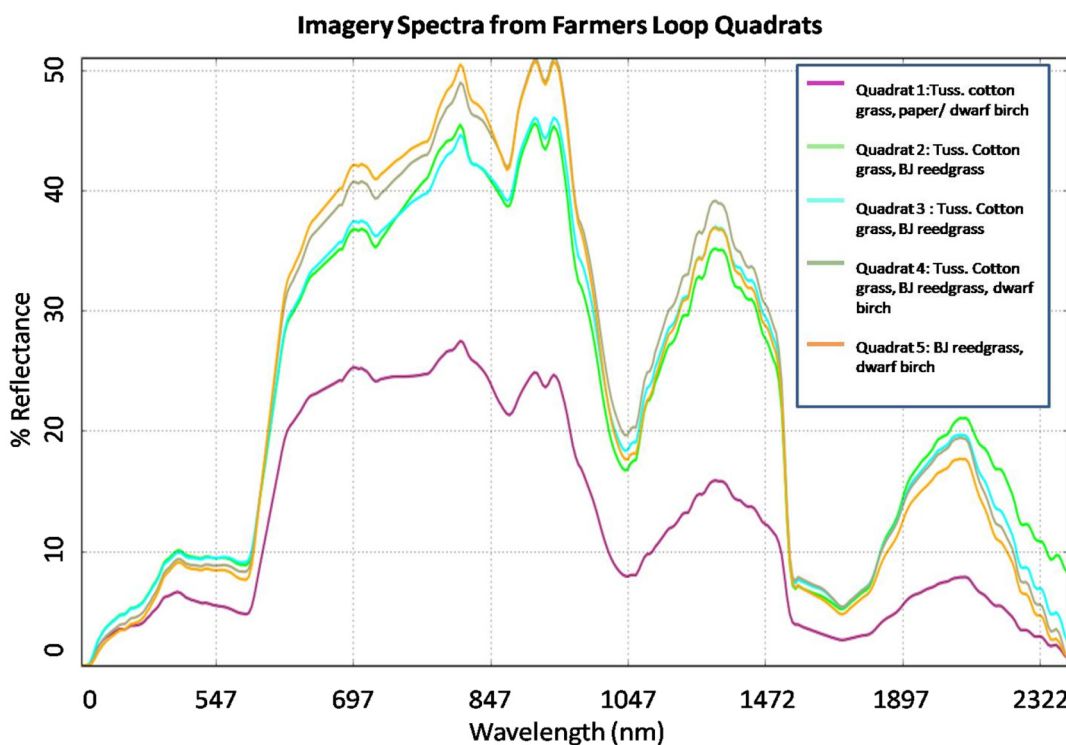


Fig. 8. Spectra extracted from the hyperspectral imagery for each quadrat at Farmers Loop used in training sample development and the SAM classification.

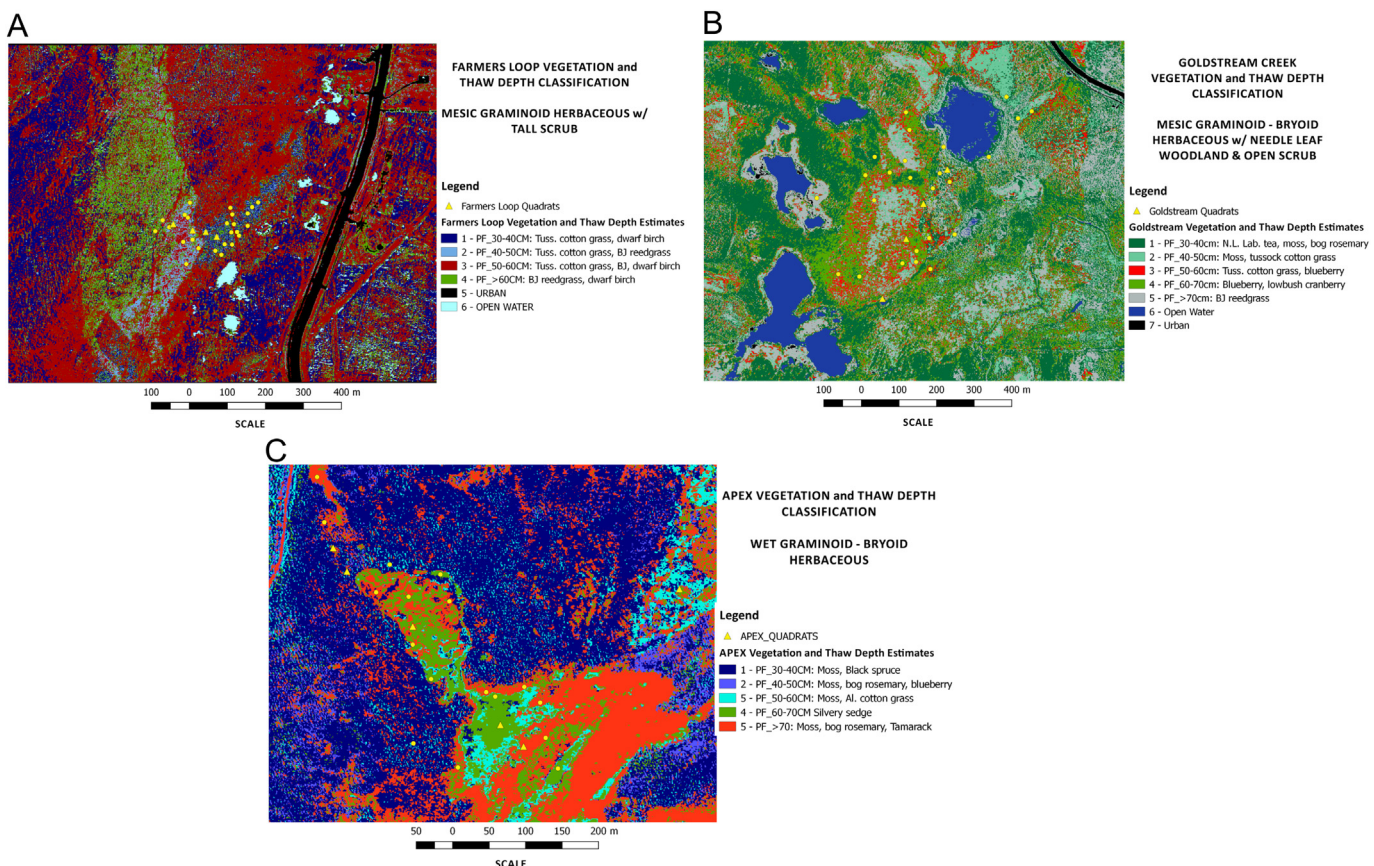


Fig. 9. Vegetation and July thaw depth estimate maps produced from the hyperspectral imagery for each of the three sites: A-Farmers Loop, B-Goldstream Creek, and C-APEX.

the height of the growing season. Farmers Loop also had significantly higher ($P < 0.0001$) pH values and the most reducing conditions (typical in wetlands) in the standing water between the tussock mounds of the sites tested.

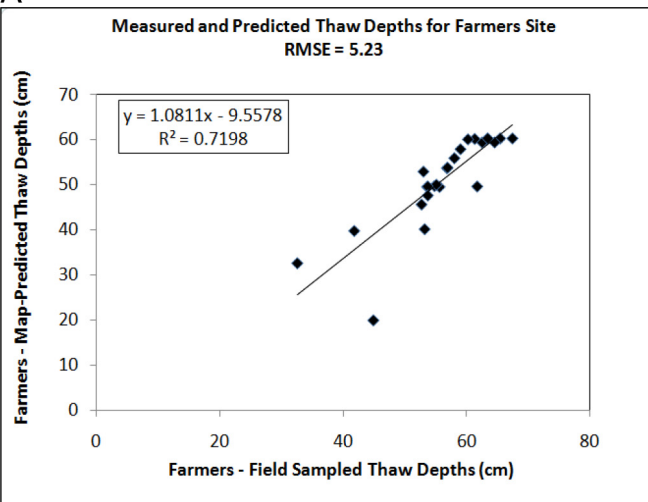
The CCA analysis of the quadrats at Farmers Loop showed a strong association between the sample quadrats and vegetation types – aligning along a pH gradient that was inversely related to the Eh gradient. Dominant vegetative features included: willow, blueberry, birch and grasses. Spectrally, this site had lower overall reflectance values, due in part to the moist, peat-filled spaces mentioned that attenuated the near and short-wave infrared regions. For the six classes developed for Farmers Loop, overall map accuracy resulted in 87% the average *producer's* error (how well a certain area is classified) was 78% and average *user's* error was 84%. These results indicated some categories such as classes 2 and 4 (tussock cotton grass and bluejoint reedgrass) had 52% and 67% of the pixels correctly classified as those categories on the ground. This is demonstrative of class separation scores typically encountered in complex vegetation morphologies (Ustin et al., 2004). The thaw prediction model for Farmers Loop resulted in an r^2 of 0.71 and a computed standard deviation of the residuals (RMSE) of 5.23 cm. Given the range of depths at this site, this translated into a map prediction error of 8 to 15% of the lowest and highest field-checked values. It is also important to note that the RMSE also fell well within the standard deviation of the seasonal thaw depth measurements for Farmers Loop (9 cm) obtained from 2014 to 2017.

Goldstream Creek was wetter with numerous closed ponds at the margins of the study site, consisting of a broad area of moss, tussock and shrubs with intermittent, widely spaced black and white spruce rising over a dome that is 0.5 to 1.0 m in elevation along the 300 m transect. Despite the wetter conditions, soils across the Goldstream Creek transect were less reducing than those across the Farmers Loop

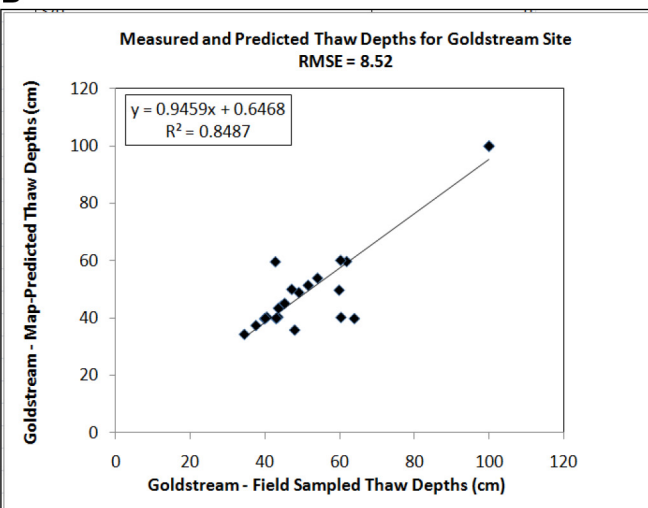
transect. The CCA analysis for this site found the vegetation associations and environmental variables falling between the Farmers (Mesic Graminoid) and APEX (Wet Graminoid-Bryoid) sites, reflecting the transitional nature of the site. The major plants observed across the Goldstream Creek transect included black spruce, Labrador tea, blueberry, and cloudberry with one vegetation class associated with > 70 cm thaw depths. Class separation scores were the best of the three sites. Overall classification accuracy was 86% with average users and producer's accuracies of 85% and 94%. User accuracy for the tussock cotton grass and blueberry category was lowest at 41% – lower than the user's accuracy seen in the Farmers Loop tussock class data. The Goldstream error analysis between the measured and predicted data resulted in an r^2 of 0.84 and an RMSE of 8.52 cm. The depth range error for Goldstream was 15 to 37% of the map-predicted and field measured values and the Goldstream's site's map-predicted thaw depths fell within the standard deviation of our yearly field measurements (12.67 cm).

The sample transects at APEX included elevated wooded areas transitioning into a considerably wetter, semi-permanently flooded bog featuring a perched water table and floating mat of moss and peat. APEX is characteristic of a ‘quaking’ bog dominated by *Sphagnum* bounded by spruce and tamarack. This site recorded the deepest thaw depths of all the sites – with some depths well beyond 1.5 m. CCA analysis showed APEX independent of the other two sites and associated with thaw depth and gravimetric water content variables reflecting its wet nature (Fig. 7). Five classes were developed for APEX with all but one containing moss as a component of the vegetation complex. Overall accuracy of the classification was 85% with users and producers accuracies averaging 82% and 85%, respectively. The thaw prediction model produced for APEX resulted in an r^2 of 0.78 and an RMSE of 10.88 cm. APEX resulted in the highest RMSE for many depths at or just exceeding 100 cm. APEX offered a predictive range error of 15

A



B



C

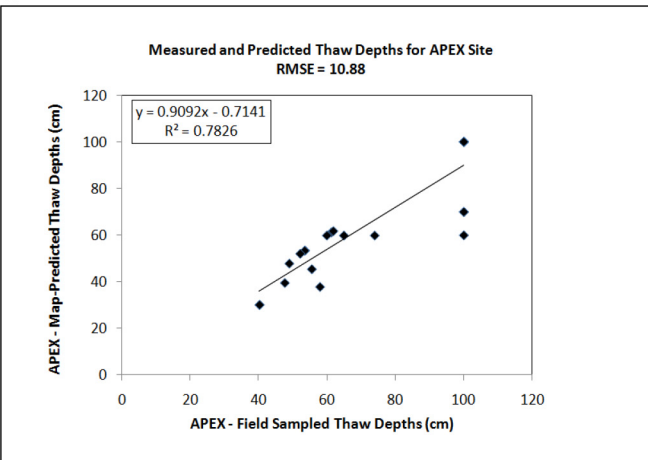


Fig. 10. Prediction models and error computed for field-measured check points ($n = 25$) and corresponding map-predicted depths and RMSE (cm) for each site.

to 37% agreement between map-predicted and field measured depth values. The predicted depths for this site barely fell within the standard deviation of the yearly measurements at 13.2 cm. The dominance of moss and open water contributed to deeper thaw depths serving as evidence of areas in Alaska where tussock, trees and shrub communities

Table 5

Summary model statistics for measured and predicted thaw depths at each site including the percent range error between low and high predicted and measured values.

Site	R ²	RMSE(cm)	% Range of field-checked values
Farmers Loop	0.71	5.23	8 to 15
Goldstream	0.84	8.52	15 to 37
APEX	0.78	10.88	15 to 37

are being replaced by wetland-dominated communities (Walker et al., 2003).

4. Discussion

Vegetation ecological relationships in discontinuous permafrost terrains in Interior Alaska have been shown to associate with changes in increased climatic warming, seasonal thaw, and soil hydro-biological changes (Walker et al., 2003; Christensen et al., 2004). In relating vegetation composition and thaw depth we found stark differences in the depth of the active layer as related to terrain and cover types. In fact, many studies emphasize that not only is the areal extent of permafrost shrinking due to thaw, but the depth of the seasonally thawed active layer is increasing (Lawrence and Slater, 2005; Brown et al., 2015; Pastick et al., 2015; Jorgenson et al., 2010). Earlier work in Canadian permafrost peatlands showed that species composition largely controlled seasonal thaw and in Interior Alaska, where current mean annual temperature (MAT) of -1°C is expected to experience an increase in MAT of 2–5 °C by 2100, vegetation composition changes are very likely (Douglas et al., 2014; Finger et al., 2016; Camill, 1999).

Results from this study infer vegetation-seasonal thaw relationships could be applied toward a better understanding of how and where “ecosystem protection,” (as offered by Shur and Jorgenson (2007)), allows permafrost to be stable in relatively warm areas such as interior Alaska. Our study found similar relationships with some vegetation-thaw depth relationships being stronger than others with our analysis identifying tussock terrains (i.e., Farmers Loop) as having the best classification and modeling results. For example, tussocks tend to grow over thick organic and ice rich soils and in poorly drained areas (Jorgenson et al., 2001b). They also may provide the strongest thermal protection of permafrost with tussock terrains near our study sites characterized by permafrost temperatures that are $\sim 3^{\circ}\text{C}$ colder than mid-successional birch and spruce stands (Dingman and Koutz, 1974). As such, an improved remotely sensed capability to identify tussock vegetation could provide information on more resilient permafrost terrains.

Finally, it is important to consider other (holistic) variables not considered at this stage of our investigation, namely snowpack characteristics, vegetative albedo, soil heterogeneities, and temperature effects (Loranty et al., 2018; Asner, 1998). Our reflectance measurements showed distinct differences in (near infrared reflectance) for each site related to biomass composition. While considering other biophysical variables linked to vegetation community development (e.g., pH, soil substrate, water content) as suggested by Lafleur (2008), canopy albedo has been shown to exert control on active layer thaw and thus could prove to be an important predictive variable for any future mapping technique (Blok et al., 2011).

5. Conclusions

In this study we explored three distinct sites three vegetation ecological classification regimes during the height of the current, local growing season. For each of the three types investigated: Mesic Graminoid Herbaceous (Farmers Loop), Mesic Graminoid-Bryoid Herbaceous (Goldstream Creek), and Wet Graminoid-Bryoid

Herbaceous (APEX), the combination of rigorous field data and analytical methods showed each site was associated with vegetation types that could be spectrally characterized (using a distance classifier) and classified with statistical association to thaw depth. From this we developed detailed, local site maps of thaw depth based on vegetation-thaw relationships and regression models representing predicted versus field-measured depths. Finally, we assessed the strength of the models using error analysis to show the range of confidence each model possessed per site. Additionally, it was demonstrated that these data could be extrapolated up to 1 km² from the sampling sites.

We feel refinement of the technique including additional sensor capabilities and spatial and temporal data as well as the use of seasonal vegetation patterns (acquired during the local growing season) could provide much needed information on the remote estimation of seasonal thaw depths in denied permafrost terrains. In addition, recent classification techniques based on machine learning that can ingest disparate, ancillary data sources such as support vector machine (SVM) and Random Forest should be investigated. SVM has been recently shown to be highly effective in increasing vegetation classification accuracies in areas of high species (and feature spectral) heterogeneity by combining data such as LiDAR with multi- and hyperspectral imagery (Ham et al., 2005; Zhang, 2014). Over time, this could allow for multi-sensor, multi-resolution remote assessment of permafrost resilience or vulnerability to climate warming or disturbance.

Funding

This project was funded by the U.S. Army Engineer Research and Development Center's Army 6.1 Basic Research Program. Support for field measurements came from the Department of Defense's Strategic Environmental Research and Development Program (Projects RC-2110 and RC18-C2-1170). NASA's Arctic Boreal Vulnerability Experiment is acknowledged for collaborative support.

Acknowledgements

This project was funded by the U.S. Army Engineer Research and Development Center's 6.1 Basic Research Program and the Strategic Environmental Resource and Development Program (project RC18-1170). We thank Merritt Turetsky for access to the APEX field site and information on conditions and datasets there. The Farmer's Loop Experimental Station is operated by the U.S. Army Cold Regions Research and Engineering Laboratory. Field assistance from Tara Anderson, Amanda Barker, Samuel Beal, Elias Deeb, Arthur Gelvin, Emilia Grzesik, Anna Wagner, Ricky Massaro, and Simone Whitecloud is greatly appreciated.

References

- Anderson, J.E., Barbato, R.A., Douglas, T.A., Newman, S.D., 2016. Variability in permafrost depth and potential biogeochemical indicators in Alaskan peatlands. In: Proceedings of the 101st Annual Meeting and Exposition of the Ecological Society of America, Fort Lauderdale, Florida, USA, 7–12 August, pp. 44.
- Asner, G.P., 1998. Biophysical and biochemical sources of variability in canopy reflectance. *Remote Sens. Environ.* 64, 234–253. [https://doi.org/10.1016/S0034-4257\(98\)00014-5](https://doi.org/10.1016/S0034-4257(98)00014-5).
- Ball Aerospace, 2008. OPTICKS Open Source Spectral Processing Software. Retrieved from. <http://opticks.org>.
- Barbour, M.G., Burk, J.H., Pitts, W.D., 1987. *Terrestrial Plant Ecology*, 2nd ed. Benjamin – Cummings, Menlo Park, CA, USA, pp. 182–223 (ISBN 0-8053-0541-6).
- Blok, D., Schaepman-Strub, G., Bartholomeus, H., Heijmans, M.P.D., Maximov, T., Berendse, F., 2011. The response of Arctic vegetation to the summer climate: relation between shrub cover, NDVI, surface albedo and temperature. *Environ. Res. Lett.* 6 (035502). <https://doi.org/10.1088/1748-9326/6/3/035502>. (9pp).
- Bohrerova, Z., Stralkova, R., Posesvova, J., Bohrer, G., Pokorny, E., 2004. The relationship between redox potential and nitrification under different sequences of crop rotations. *Soil Tillage Res.* 2004 (77), 25–33. <https://doi.org/10.1016/j.still.2003.10.006>.
- Bouchard, F., Macdonald, L., Turner, K., Thienpont, J., Medeiros, A., Biskaborn, B., Korosi, J., Hall, R., Pienitz, R., Wolfe, B., 2016. Paleolimnology of thermokarst lakes: a window into permafrost landscape evolution. *Arctic Sci* 3, 91–117. <https://doi.org/10.1139/as-2016-0022.2016>.
- Brewer, R., 1979. *Principles of Ecology*. Holt, Rhinehart and Winston, Orlando, FL, USA, 0-7216-1988-6pp. 165–172.
- Brown, D.R.N., Jorgenson, M.T., Douglas, T.A., Romanovsky, V., Kielland, K., Euskirchen, E., 2015. Vulnerability of permafrost to fire-initiated thaw in lowland forests of the Tanana Flats, interior Alaska. *J. Geophys. Res. Biogeosci.* <https://doi.org/10.1002/2015JG003033>. 19 pages.
- Camill, P., 1999 Oct 16. Patterns of boreal permafrost peatland vegetation across environmental gradients sensitive to climate warming. *Can. J. Bot.* 77 (5), 721–733.
- Campbell, James B., Wynne, Randolph H., 2011. *Introduction to Remote Sensing*. Guilford Press, New York, NY, USA, 978-1-60918-176-5pp. 408–418.
- Chapman, W.L., Walsh, J.E., 2007. A synthesis of Antarctic temperatures. *J. of Clim.* 20, 4096–4117. <https://doi.org/10.1175/JCLI4236.1.2007>.
- Christensen, T.R., Johansson, T., Akerman, H.J., Mastepanov, M., Malmer, N., Friberg, T., Crill, P., Svansson, B.H., 2004. Thawing sub-arctic permafrost: effects on vegetation and methane emissions. *Geophys. Res. Lett.* 31 (L04501), 1–4 DOI:10.1029/2003GL018680.
- Christiansen, T., Johansson, T., Akerman, H.J., Mastepanov, M., 2012. Thawing sub-arctic permafrost: effects on vegetation and methane emissions. *Geophys. Res. Lett.* 31 (L04501), 1–4. <https://doi.org/10.1029/2003GL018680>.
- Congalton, R.G., 1991. A review of assessing the accuracy of classifications of remotely sensed data. *Remote Sens. Environ.* 37, 35–46. [https://doi.org/10.1016/0034-4257\(91\)90048-B](https://doi.org/10.1016/0034-4257(91)90048-B).
- Congedo, L., 2016. Semi-automatic classification plugin. Documentation. <https://doi.org/10.13140/RG.2.2.29474.02242/1>.
- Cowardin, L.M., Carter, V., Golet, F.C., LaRoe, E.T., 1979. *Classification of Wetlands and Deep Water Habitats of the United States*. US Government Printing Office FWS/OBS-79/31, US Fish and Wildlife Service.
- Dingman, S., Koutz, F., 1974. Relations among vegetation, permafrost, and potential isolation in central Alaska. *Arct. Alp. Res.* 6 (1), 37–47. <https://doi.org/10.2307/1550368>.
- Douglas, T.A., Jones, M.C., Hiemstra, C.A., Arnold, J.R., 2014. Sources and sinks of carbon in boreal ecosystems of interior Alaska: a review. *Elem Sci Anth.* 2, 32. <https://doi.org/10.12952/journal.elementa.000032>. 2014.
- Douglas, T.A., Jorgenson, M.T., Brown, D.R.N., Campbell, S.W., Hiemstra, C.A., Saari, S.P., Bjella, K., Liljeblad, A.K., 2016. Degrading permafrost mapped with electrical resistivity tomography, airborne imagery and LiDAR, and seasonal thaw measurements. *Geophysics* 81 (1). <https://doi.org/10.1190/GEO2015-0149.1>.
- Drenovsky, R.E., Vo, D., Graham, K.J., Scow, K.M., 2004. Soil water content and organic carbon availability are major determinants of soil microbial community composition. *Microb. Ecol.* 48 (3), 424–430.
- Duguay, C., Zhang, T., Leverington, D., Romanovsky, V., 2005. Satellite remote sensing of permafrost and seasonally frozen ground. In: *Remote Sensing of Northern Hydrology* Geophysical Monograph Series 163. The American Geophysical Union. <https://doi.org/10.1029/163GM06>.
- Dumbrell, A.J., Nelson, M., Helgason, T., Dytham, C., Fitter, A.H., 2010. Relative roles of niche and neutral processes in structuring a soil microbial community. *ISME J.* 4 (3), 337.
- Eckert, L., Sims, J.T., 2011. Recommended soil pH and lime requirement tests. In: Sims, J.T., Wolf, A. (Eds.), *Recommended Soil Testing Procedures for the Northeastern United States*. Northeast Regional Bulletin #493, 3rd edition. Agricultural Experiment Station, University of Delaware, Newark, DE, pp. 19–25.
- Finger, R.A., Turetsky, M.R., Kielland, K., Ruess, R.W., Mack, M.C., Euskirchen, E.S., 2016. Effects of permafrost thaw on nitrogen availability and plant-soil interactions in a boreal Alaskan lowland. *J. Ecol.* 104 (6), 1542–1554.
- Fisher, J.B., Hayes, D.J., Schwalm, C.R., Huntzinger, D.N., Stofferahn, E., Schaefer, K., Luo, Y., Wullschleger, S.D., Goetz, S., Miller, C.E., Griffith, P., 2018. Missing pieces to modeling the Arctic-Boreal puzzle. *Environ. Res. Lett.* 13 (2), 020202.
- Gorham, E., 1967. Some chemical aspects of wetland ecology. In: *Tech. Memorandum-Committee on Geotechnical Research*, NRC of Canada No 90, pp. 20–38.
- Hachem, S., Allard, M., Duguay, C., 2009. Using the MODIS land surface temperature product for mapping permafrost: an application to northern Québec and Labrador, Canada. *Periglac. Process.* 20, 407–416. <https://doi.org/10.1002/pp.672>.
- Ham, J., Chen, Y., Crawford, M.M., Ghosh, J., 2005. Investigation of the Random Forest framework for classification of hyperspectral data. *IEEE Trans. Geosci. Remote Sens.* 43, 492–501. <https://doi.org/10.1109/TGRS.2004.8390924>.
- Hodgkins, S.B., Tfaily, M.M., McCalley, C.K., Logan, T.A., Crill, P.M., Saleska, S.R., Rich, V.I., Chanton, J.P., 2014. Changes in peat chemistry associated with permafrost thaw increase greenhouse gas production. *Proc. Natl. Acad. Sci.* 111 (16), 5819–5824.
- Husson, O., 2013. Redox potential (Eh) and pH as drivers of soil/plant/microorganism systems: a transdisciplinary overview pointing to integrative opportunities for agronomy. *Plant Soil* 362, 389–417. <https://doi.org/10.1007/s11007-012-1429-7>.
- Jensen, R., Mausel, P., Dias, N., Gonser, R., Yang, C., Everitt, J., Fletcher, R., 2007. Spectral analysis of coastal vegetation and land cover using AISA + hyperspectral data. *Geocarto Int* 22, 17–28. <https://doi.org/10.1080/10106040701204354>.
- Jones, B.M., Stoker, J.M., Gibbs, A.E., Grosse, G., Romanovsky, V.E., Douglas, T.A., Kinsman, N.E., Richmond, B.M., 2013. Quantifying landscape change in an arctic coastal lowland using repeat airborne LiDAR. *Environ. Res. Lett.*, vol. 8, 045025. <https://doi.org/10.1088/1748-9326/8/4/045025>.
- Jongman, R.H.G., Ter Braak, C.J.F., Van Tongeren, O.F.R., 1986. *Data Analysis in Community and Landscape Ecology*. Cambridge University Press, Cambridge, United Kingdom, 0-521-47574-0pp. 137–144.
- Jorgenson, M.T., Racine, C.H., Walters, J.C., 2001a. Permafrost degradation and ecological changes associated with a warming climate in Central Alaska. *Clim. Chang.* 48, 551. <https://doi.org/10.1023/A:1005667424292>.
- Jorgenson, M.T.; Racine, C.H.; Walters, J.C.; and Osterkamp, T.E. Permafrost degradation

- and ecological changes associated with a warming climate in central Alaska. *Clim. Chang.* 2001b, 48: 551. DOI:<https://doi.org/10.1023/A:1005667424292>.
- Jorgenson, M., Romanovsky, V., Harden, J., Shur, Y., O'Donnell, J., Schuur, E., Kanevskiy, M., Marchenko, S., 2010. Resilience and vulnerability of permafrost to climate change. *Can. J. For. Res.* 40, 1219–1236. <https://doi.org/10.1139/X10-060>.
- Karpouzli, E., Malthus, T., 2003. The empirical line method for the atmospheric correction of IKONOS imagery. *Int. J. Remote Sens.* 24 (5), 1143–1150. <https://doi.org/10.1080/014311602100026779>.
- Kreig, R.A., Reger, R.D., 1982. Air-photo analysis and summary of landform soil properties along the route of the trans-Alaska pipeline system. In: Alaska Division of Geological & Geophysical Surveys Geologic Report. vol. 66. pp. 149. <https://doi.org/10.14509/426>.
- Kruse, F.A., Lefkoff, A.B., Boardman, J.W., Heidebrecht, K.B., Shapiro, A.T., Barloon, J.P., Goetz, A.F.H., 1993. The spectral image processing system (SIPS) - interactive visualization and analysis of imaging spectrometer data. *Remote Sens. Environ.* 44, 145–163.
- Kuuluvainen, Timo, Hokkanen, Timo J., Järvinen, Erkki, Pukkala, Timo, 1993. Factors related to seedling growth in a boreal Scots pine stand: a spatial analysis of a vegetation-soil system. *Can. J. For. Res.* 23 (10), 2101–2109.
- Kuzyakov, Y., Xu, X., 2013. Competition between roots and microorganisms for nitrogen: mechanisms and ecological relevance. *New Phytol.* 198, 656–669. <https://doi.org/10.1111/nph.12235>.
- Lafleur P M and Humphreys E R 2008 Spring warming and carbon dioxide exchange over low Arctic tundra in central Canada *Glob. Change Biol.* 14 740–56. DOI:<https://doi.org/10.1111/j.1365-2486.2007.01529>.
- Lawrence, D.M., Slater, A.G., 2005. A projection of severe near-surface permafrost degradation during the 21st century. *Geophys. Res. Lett.* 32, L24401. <https://doi.org/10.1029/2005GL025080>.
- Loranty, M.M., Abbott, B.W., Blok, D., Douglas, T.A., Epstein, H.E., Forbes, B.C., Jones, B.M., Kholodov, A.L., Kropp, H., Malhotra, A., Mamet, S.D., 2018 May 7. Reviews and Syntheses: Changing Ecosystem Influences on Soil Thermal Regimes in Northern High-Latitude Permafrost Regions. Oak Ridge National Lab.(ORNL), Oak Ridge, TN (United States).
- Mackelprang, R., Burkert, A., Haw, M., Mahendrarajah, T., Conaway, C.H., Douglas, T.A., Waldrop, M.P., 2017. Microbial survival strategies in ancient permafrost: insights from metagenomics. *ISME J.* <https://doi.org/10.1038/nature10576>.
- Marschner, Petra, Yang, C.-H., Lieberei, Reinhard, Crowley, David E., 2001. Soil and plant specific effects on bacterial community composition in the rhizosphere. *Soil Biol. Biochem.* 33 (11), 1437–1445.
- McGuire, A. D., M. Sturm, and F. S. Chapin III. Arctic Transitions in the Land–Atmosphere System (ATLAS): background, objectives, results, and future directions, *J. Geophys. Res.* 2003, 108, 8166, DOI:10.1029/2002JD002367, D2.
- McPartland, M., Falkowski, M., Reinhardt, J., Kane, E., Kolka, R., Turetsky, M., Douglas, T., Anderson, J., Edwards, J., Reinhardt, J., Palik, B., Montgomery, R., 2019. Characterizing boreal peatland plant composition and species diversity with hyperspectral remote sensing. *J. Remote Sens. Soc.* 2018, 10 (Accepted paper).
- Mitch, W.J., Gosselink, J.G., 1986. Wetlands. Van Nostrand Rhinehold, New York, NY, USA, 0-442-26398-8pp. 287–315.
- Moore, P.D., Bellamy, D.J., 1974. Peatlands. Springer-Verlag, New York, NY, USA, 978-1-4684-6293-7pp. 221.
- Morrissey, L.A., Strong, L.L., Card, D.H., 1986. Mapping permafrost in the boreal forest with thematic mapper satellite data. *Photogramm. Eng. Remote. Sens.*(0099-1112) 52 (1513–152).
- Osterkamp, T.E., Jorgenson, M.T., Schuur, E.A.G., Shur, Y.L., Kanevskiy, M.Z., Vogel, J.G., Tumskoy, V.E., 2009. Physical and ecological changes associated with warming permafrost and thermokarst in interior Alaska. *Permafro. Periglac. Process.* 20, 235–256. <https://doi.org/10.1002/pp.656>.
- Pastick, N.J., Jorgenson, M.T., Wylie, B.K., Nield, S.J., Johnson, K.D., Finley, A.O., 2015. Distribution of near-surface permafrost in Alaska: estimates of present and future conditions. *Remote Sens. Environ.* 168, 301–315.
- Peddle, D.R., Franklin, S.E., 1993. Classification of permafrost active layer depth from remotely sensed and topographic evidence. *Remote Sens. Environ.* 44 (1), 67–80. [https://doi.org/10.1016/0034-4257\(93\)90103-5](https://doi.org/10.1016/0034-4257(93)90103-5).
- Perry, E.M., Warner, T., Foote, P., 2000. Comparison of atmospheric modeling versus empirical line fitting for mosaicking HYDICE imagery. *Int. J. Remote Sens.* 21 (4), 799–803. <https://doi.org/10.1080/01431160210588>.
- Sasaki, K., Kawata, S., Minami, S., 1983. Constrained nonlinear method for estimating component spectra from multicomponent mixtures. *Appl. Opt.* 22 (22), 3599–3603.
- Satterwhite, M.B., Henley, J.P., 1990. Hyperspectral Signatures (400 to 2500 nm) of Vegetation, Minerals, Soils, Rocks, and Cultural Features: Laboratory and Field Measurements. US Army Corps of Engineers, Engineer Topographic Laboratories-0573. USAETL, Fort Belvoir, Virginia, USA.
- Schuur, E.A., Crummer, K.G., Vogel, J.G., Mack, M.C., 2006. Plant species composition and productivity following permafrost thaw and thermokarst in Alaskan tundra. *Ecosystems* 10, 280–292. <https://doi.org/10.1038/nature08031>.
- Shur, Y.L., Jorgenson, M.T., 2007. Patterns of permafrost formation and degradation in relation to climate and ecosystems. *Permafro. Periglac. Process.* 18, 7–19. <https://doi.org/10.1002/pp.582.2007>.
- Sluiter, R., Pebesma, E.J., 2010. Comparing techniques for vegetation classification using multi- and hyperspectral images and ancillary environmental data. *Int. J. Remote Sens.* 31 (23), 0143–1161. <https://doi.org/10.1080/01431160903401379>.
- Smith, G.M., Milton, E.J., 1999. Technical note: the use of the empirical line method to calibrate remotely sensed data to reflectance. *Int. J. Remote Sens.* 20. <https://doi.org/10.1080/014311699211994>.
- Smith, M.O., Johnson, P.E., Adams, J.B., 1985. Quantitative determination of mineral types and abundances from reflectance spectra using principal components analysis, Lunar and Planetary Institute, NASA, American Geophysical Union, et al., Lunar and Planetary Science Conference, 15th, Houston, TX, Mar. 12–16, 1984. *J. Geophys. Res.* 90, C797–C804 Supplement (ISSN 0148-0227). Feb. 15.
- Soil Survey Staff, 2009. In: Burt, R. (Ed.), *Soil Survey Field and Laboratory Methods Manual*. Soil Survey Investigations Report No. 51, Version 1.0. U.S. Department of Agriculture, Natural Resources Conservation Service.
- Ter Braak, C.J.F., 1986. Canonical correspondence analysis: a new eigenvector technique for multivariate direct gradient analysis. *Ecology* 67 (5), 1167–1179. <https://doi.org/10.2307/1938672>.
- Ustin, S.L., Roberts, D.A., Gamon, J.A., Asner, G.P., Green, R.O., 2004. Using imaging spectroscopy to study ecosystem processes and properties. *Bioscience* 54 (6), 523–534. [https://doi.org/10.1641/0006-3568\(2004\)054\[0523:UITSE\]2.0.CO;2](https://doi.org/10.1641/0006-3568(2004)054[0523:UITSE]2.0.CO;2).
- Viereck, L.A., Dyrness, C.T., Batten, A.R., and Wenzlick, K.J. The Alaska Vegetation Classification. Gen. Tech. Rep. PNW-GTR-286. Portland, OR: U.S. Department of Agriculture, Forest Service, Pacific Northwest Research Station. (278 p.).
- Walker, D.A., Jia, G.J., Epstein, H.E., Raynolds, M.K., Chapin III, F.S., Copass, C., Hinzman, L.D., Knudson, J.A., Maier, H.A., Michaelson, G.J., Nelson, F., Ping, L., Romanovsky, V.E., Shiklomanov, N., 2003. Vegetation-soil-thaw-depth relationships along a low-Arctic bioclimate gradient, Alaska: synthesis of information from the ATLAS studies. *Permafro. Periglac. Process.* 14, 103–123. <https://doi.org/10.1002/pp.452>.
- Walker, M.D., Wahrenb, C.H., Hollister, R.D., Henry, G.H., Ahlquist, L.E., Atalo, J.M., Bret-Harte, M.S., Calef, M.P., Callaghan, T.V., Carroll, A.B., Epstein, H.E., Jónsdóttir, I.S., Klein, J.A., Magnusson, B., Molau, U., Oberbauer, S.F., Rewa, S.P., Robinson, C.H., Shaver, G.R., Suding, K.N., Thompson, C.G., Tovanan, A., Totland, Ø., Turner, P.L., Tweedie, C.E., Webber, P.J., Wooley, P.A., 2006. Plant community responses to experimental warming across the tundra biome. *Proc. Natl. Acad. Sci. U. S. A.* 103, 1342–1346. <https://doi.org/10.1073/pnas.0503198103>.
- Wilhelm, R.C., Niederberger, T.D., Greer, C., Whyte, L.G., 2011. Microbial diversity of active layer and permafrost in an acidic wetland from the Canadian High Arctic. *Can. J. Microbiol.* 57 (4), 303–315. <https://doi.org/10.1139/w11-004>.
- Wolken, J. M.; Hollingsworth, T.N.; Rupp, T.S.; Chapin III, F.S.; Trainor, S.F.; Barrett, T.M. ; Sullivan, P.F.; McGuire, A.D.; Euskirchen, E. S.; Hennon, P.E.; Beever, E.A.; Conn, J. S.; Crone, L.K.; D'Amore, D.V.; Fresco, N.; Hanley, T.A.; Kielland, K.; Kruse, J.J.; Patterson, T. and Yarie, J. Evidence and implications of recent and projected climate change in Alaskas forest ecosystems. *Ecosphere* 2011. 2(11):124. DOI:<https://doi.org/10.1890/ES11-00288.1>.
- Xue, K., Mengting, M.Y., Zhou, J.S., Yujia, Q., Ye, D., Lei, C., Liyou, W., Zhili, H., Van Nostrand, J.D., Bracho, R., Natali, S., Schuur, E.A.G., Chengwei, L., Konstantinidis, K.T., Qiong, W., Cole, J.R., Tiedje, J.M., Yiqi, L., Jizhong, Z., 2016. Tundra soil carbon is vulnerable to rapid microbial decomposition under climate warming. *Nat. Clim. Chang.* 06, 595–600. Nature Publishing Group 1758-678X. <https://doi.org/10.1038/nclimate2940>.
- Zak, D.R., Kling, G.W., 2006. Microbial community composition and function across an Arctic TundraLandscape. *Ecology* 87, 1659–1670. [https://doi.org/10.1890/0012-9658\(2006\)87\[1659:MCCAF\]2.0.CO;2](https://doi.org/10.1890/0012-9658(2006)87[1659:MCCAF]2.0.CO;2).
- Zhang, C., 2014. Combining hyperspectral and lidar data for vegetation mapping in the Florida Everglades. *PE&RS* (8), 733–743. <https://doi.org/10.14358/PERS.80.8.733>.